



HAL
open science

Structural and mechanistic insights into type II trypanosomatid tryparedoxin-dependant peroxidases

Magnus S Alpey, Janine Konig, Alan H Fairlamb

► **To cite this version:**

Magnus S Alpey, Janine Konig, Alan H Fairlamb. Structural and mechanistic insights into type II trypanosomatid tryparedoxin-dependant peroxidases. *Biochemical Journal*, 2008, 414 (3), pp.375-381. 10.1042/BJ20080889 . hal-00479020

HAL Id: hal-00479020

<https://hal.science/hal-00479020>

Submitted on 30 Apr 2010

HAL is a multi-disciplinary open access archive for the deposit and dissemination of scientific research documents, whether they are published or not. The documents may come from teaching and research institutions in France or abroad, or from public or private research centers.

L'archive ouverte pluridisciplinaire **HAL**, est destinée au dépôt et à la diffusion de documents scientifiques de niveau recherche, publiés ou non, émanant des établissements d'enseignement et de recherche français ou étrangers, des laboratoires publics ou privés.

Structural and mechanistic insights into type II trypanosomatid tryparedoxin-dependant peroxidases

Magnus S. ALPHEY¹, Janine KÖNIG¹, Alan H. FAIRLAMB²

Division of Biological Chemistry & Drug Discovery, College of Life Sciences, University of Dundee, Dundee, DD1 5EH, UK.

Short title: Structure of *T. brucei* tryparedoxin-dependant peroxidase

Abbreviations used: TryX, tryparedoxin; TDPX, tryparedoxin-dependent peroxidase; GPX, glutathione peroxidase; PEG, polyethylene glycol; r.m.s.d., root mean square deviation
Model coordinates and structure factors have been deposited with the PDB under accession code 2VUP.

¹These authors contributed equally to this work

²To whom correspondence should be addressed (email a.h.fairlamb@dundee.ac.uk)

Synopsis

Trypanosoma brucei tryparedoxin-dependant peroxidase (*TbTDPX*) is a genetically validated drug target in the fight against African sleeping sickness. Despite its similarity to members of the glutathione peroxidase (GPX) family, *TbTDPX2* is functional as a monomer, lacks a selenocysteine residue, relying instead on peroxidatic and resolving cysteines for catalysis and uses tryparedoxin rather than glutathione as electron donor. Kinetic studies indicate a saturable ping-pong mechanism, unlike selenium-dependent GPXs which display infinite K_m and V_{max} values. The structure of the reduced enzyme at 2.1 Å-resolution reveals that the catalytic thiol groups are widely separated (19 Å) and thus unable to form a disulphide bond without a large conformational change in the secondary structure architecture, as reported for certain plant GPXs. A model of the oxidized enzyme structure is presented and the implications for small molecule inhibition are discussed.

Key words: Dithiol-dependent peroxidase; drug discovery; glutathione peroxidase; *Leishmania*; *Trypanosoma*; trypanothione

INTRODUCTION

Human African trypanosomiasis (sleeping sickness) is responsible for an estimated 80,000 new cases and 30,000 deaths each year [1]. Current therapeutics against the protozoan parasite (*Trypanosoma brucei* spp) are inadequate and new drugs are urgently needed [2]. Much research has focussed on the unique thiol metabolism of trypanosomes, centred around the metabolite trypanothione (N^1, N^8 -bis(glutathionyl)spermidine) [3]. The trypanothione peroxidase system prevents damage by oxidative stress by reduction of peroxides via NADPH, trypanothione reductase, trypanothione, tryparedoxin (TryX) and tryparedoxin peroxidase, a 2-Cys peroxiredoxin. All components of this cascade are essential for parasite survival [4-8].

Recently, a new member of this antioxidant defence system has been identified and characterized in *T. brucei* [9-11], *T. cruzi* [12] and *L. major* [13]. These tryparedoxin-dependent peroxidases (TDPXs) show highest homology to the monomeric phospholipid glutathione peroxidase (GPX4) among the mammalian proteins. However, glutathione is not a physiological substrate for these TDPXs, which use TryX, a thioredoxin-like protein, as an electron donor. Moreover, the active-site selenocysteine in GPXs is replaced by cysteine for reduction of a broad range of hydroperoxides including hydrogen peroxide and complex lipid hydroperoxides. A resolving cysteine missing in all human GPXs is essential for regeneration by TryX. The essentiality of TDPX in *T. brucei*, shown by RNAi studies [8], together with the different reaction mechanism from the mammalian GPX suggest that TDPX could be a druggable target in these parasites.

There are three TDPXs in *T. brucei* which are localised in the mitochondrion and the cytosol [10]. Apart from putative targeting sequences at the N- and C-termini, the core of these proteins is highly conserved. Previous studies have kinetically characterized a His₆-tagged *Tb*TDPX3 which included the putative mitochondrial targeting sequence [9]. Here we have kinetically analysed the non-tagged and shorter recombinant *Tb*TDPX2 and compared the results to *Tb*TDPX3. We report the first TDPX crystal structure from a trypanosomatid, the reduced form of *Tb*TDPX2 at 2.1 Å, and present a model of the oxidized form that may assist in the future design of inhibitors against this target.

EXPERIMENTAL

Cloning, expression, purification and characterization

TbTDPX2 from strain S427 was cloned into pET15b (Novagen), expressed in *Escherichia coli* BL21(DE3)pLysS and purified as the His₆-tagged protein essentially as described for *LmTDPX1* [13].

The His₆-tag was removed with thrombin and the enzyme purified to homogeneity by chromatography on nickel Sepharose, Benzamidine Sepharose and gel filtration in 50 mM Tris buffer, pH 8.0. Assay conditions were essentially as described [9]. Briefly, peroxidase activity was measured in a total volume of 250 μ l at 25 °C containing 100 mM Tris-HCl, pH 7.6, 5 mM EDTA, 250 μ M NADPH, 5 U *T. brucei* trypanothione reductase, 100 μ M trypanothione disulphide, 5 to 12.5 μ M *T. brucei* tryparedoxin, 0.2 μ M *TbTDPX2* and 50 to 800 μ M cumene hydroperoxide. Kinetic data were analysed according to [13].

For crystallization, His₆-tagged protein was reduced with 50 mM dithiothreitol, concentrated (Vivaspin20, Sartorius) and applied to Superdex S75 26/60 (GE Healthcare) equilibrated with 10 mM Tris-HCl pH 8.0. *TbTDPX2*-containing fractions were combined, 10 mM DTT and 1 mM EDTA (final concentrations) added, and protein concentrated to 7.5 mg ml⁻¹ prior to crystallization.

Crystallization, data collection, structure solution and refinement

Crystals of His₆-tagged *TbTDPX2* were grown by the hanging drop method at 18 °C. Drops of 1 μ l protein (7.5 mg ml⁻¹) and 1 μ l reservoir solution (22 % PEG 3350, 0.1 M Tris-HCl, pH 8.0) were assembled and monoclinic crystals grew overnight (1.0 x 0.05 x 0.05 mm). Crystals were cryoprotected in 35 % PEG 3350, 0.1 M Tris-HCl, pH 8.0 and flash-cooled in a stream of nitrogen at 103 K. Data were collected at the European Synchrotron Radiation Facility, Grenoble on beamline ID14 EH4 using an ADSC QUANTUM Q315r CCD detector and at a wavelength of 0.979 Å. A single crystal was used to collect 180° of data in seven batches as it was translated along its length to avoid the effects of radiation damage. Data were processed and scaled using XDS [14] and statistics are shown in Supplementary Table S1. The crystals contain one molecule in the asymmetric unit, the space group is P2₁ with a Matthews coefficient of 2.2 Å³ / Da, and a solvent content of 44 %.

Potential structural homologue candidates were identified in PDB. Chain A of structure 2P5Q, the reduced form of *PtGPX5* [15], showing a sequence identity of 52 % was used for molecular replacement in MOLREP [16]. The solution from MOLREP underwent rigid body refinement followed by restrained refinement in REFMAC5 [17,18], giving an R_{factor} and R_{free} of 32 and 40 % respectively. Residues were mutated from the *PtGPX5* sequence to that of *TbTDPX2* using COOT [19], and further cycles of restrained refinement interspersed with electron density inspection, manual model building and manipulation and water addition were performed with REFMAC5 and COOT. All residues fall into the preferred and allowed regions of the Ramachandran plot. Surface-charge representations were prepared and visualized using PDB2SQR [20], APBS [21], and PyMOL (DeLano Scientific LLC). Refinement statistics can be found in Supplementary Table S1.

Sequence and structural alignments and modelling

Structural and sequence homologues were found using DALI [22] and BLAST searches of the PDB and SWISSPROT databases. Only one structure, 1GP1 (bovine erythrocyte GPX1; [23]) was returned by DALI as a structural homologue, with an r.m.s.d. of 1.8 Å over 159

C α -atoms. However, the BLAST search of the PDB revealed several of the GPX family, which when overlaid using LSQMAN [24,25] gave r.m.s.d. values of between 1.0 Å and 1.4 Å over more than 120 C α -atoms and sequence identities of between 29 % and 52 %. SWISS-MODEL [25] was used to prepare a structural model of the oxidized form of *Tb*TDPX2 based on the structure of oxidized *Pt*GPX5. The three-dimensional structures were visualized and analyzed with COOT and PyMOL.

Stage 2(a) POST-PRINT

RESULTS AND DISCUSSION

Kinetic analysis

Previous kinetic analyses of His₆-tagged *Tb*TDPX3 [9] showed no saturation kinetics, in contrast to that of non-tagged *Lm*TDPX1 [13]. *Tb*TDPX3 has a putative N-terminal mitochondrial targeting sequence, which together with the His₆-tag, might interfere with enzyme activity. Thus, we chose to work with the shorter *Tb*TDPX2 (Figure 1). Three independent PCRs were performed using genomic DNA from *T. brucei* strain 427 as template. All clones analysed contained two point mutations at the DNA level (C233A and T246C) in comparison to *Tb*TDPX2 in the genome reference strain (gene *Tb*927.7.1130). C233A causes a mutation (Thr78Asn) at the amino acid level, and T246C is silent (Figure 1).

Recombinant protein was expressed in *E.coli* and purified to homogeneity with and without the N-terminal His₆-tag (Supplementary Figure S1A). SDS-PAGE analysis shows that non-tagged *Tb*TDPX2, which has a predicted molecular mass of 19,168 Da, runs as a monomer in both reduced and oxidised forms (Supplementary Figure S1B). Additionally, analytical size-exclusion chromatography shows that both forms elute as single monomeric peaks with relative molecular masses of 19,600 and 25,400 for the reduced and oxidised proteins, respectively (Supplementary Figure S1C). The minor size differences observed by both methods is likely to be a result of the conformational change predicted to occur between the reduced and oxidised states outlined below.

Kinetic data for non-tagged *Tb*TDPX2 were obtained by varying hydroperoxide concentrations at several fixed TryX concentrations. Results were analysed by fitting individual data sets to the Michaelis-Menten equation to obtain V_{\max}^{app} for each concentration of TryX (Figure 2A). A double reciprocal plot of $1/V_{\max}^{\text{app}}$ versus $1/[\text{TryX}]$ gave finite values for K_m and V_{\max} (Figure 2B). Since the double reciprocal transformations of the original data set were parallel the entire data set was globally fitted by non-linear regression to the equation describing a ping-pong mechanism (Figure 2C). Similar results were found by analysis of progress curves using the integrated Dalziel equation analysed as described for *Tb*TDPX3 [9] (Supplementary Figure S2). The results of these analyses are summarised in Table 1 in comparison with published data for *Tb*TDPX3 and *Lm*TDPX1. The rate constants k_1 and k_2 for cumene hydroperoxide and TryX, respectively, are in reasonable agreement to those reported for *Tb*TDPX3 [11], except our results are compatible with finite K_m values in the micromolar range rather than infinite ones. Nonetheless, the kinetic behaviour of *Tb*TDPX2 and *Tb*TDPX3 are broadly similar and thus the N-terminal His₆-tag and N-terminal extension present in *Tb*TDPX3 does not significantly perturb kinetic behaviour. Interestingly, *Lm*TDPX1 and *Tb*TDPX2 show similar catalytic-centre activity (k_{cat}) and K_m values for cumene hydroperoxide, but differ markedly in K_m for TryX, which are at least 10 times lower for *Lm*TDPX1.

Overall structure and comparisons

The crystal structure of *Tb*TDPX2 has been solved using data to 2.1 Å and displays the well-characterised thioredoxin fold [26,27]. The structure (Figure 3) is constructed around a 7-stranded twisted β -sheet with parallel (β_3 - β_4 - β_5 - β_1) and antiparallel (β_3 - β_6 - β_7) sections sharing β_3 . The sheet is flanked by three α -helices on one side (α_1 , α_2 , α_4) and one on the other (α_3). The secondary structure begins with a loop of two 3_{10} helices (θ_1 , θ_2) separated by a β -hairpin (β_1 , β_2) followed by a β - α - β unit (β_3 - α_1 - β_4). The model contains 163 residues from Ala3 to Thr166. The His₆-affinity tag, N-terminal residues 1 and 2, and C-

terminal residues 167 to 169 could not be modelled due to weak electron density suggesting a high level of flexibility in these regions.

A BLAST search with the sequence for *TbTDPX2* returned many homologues that can be grouped with those from other trypanosomes (~70% identity), plants (~50% identity) and animals (~30% identity) (Figure 1). Only eight structural homologues were found in the Protein Data Bank : bovine erythrocyte GPX1 (1GP1), human GPX1,2,3,4,5 and 7 (2F8A; 2HE3; 2R37; 2OBI [28]; 2I3Y; 2P31), and the two poplar *PtGPX5* structures (2P5Q and 2P5R [15]). These structures were overlaid revealing that the core subunit structures were well conserved with r.m.s.d. values ranging from 1.0 Å over 155 C α atoms for hGPX4, to 1.4 Å over 148 C α atoms for hGPX3.

TbTDPX2 exhibits strong similarities to the related GPXs. Unlike the majority of GPX structures that exist as either homodimers or homotetramers in solution, *TbTDPX2* exists as a monomer (Supplementary Figure S1B and S1C). Among the human GPXs, only hGPX4 is reported to be monomeric [28]. A minor deviation from the overlaid backbones is seen in loop α 3- β 6 of *TbTDPX2* (Figure 4). Although the conformation is slightly different in GPX4, this loop is the same length in both structures and shorter than the long surface exposed loop seen in the other GPX isozymes. It has been suggested that the existence of the extended loop in other GPXs limits accessibility to the active site [28], and the short loop in hGPX4 and *TbTDPX2* may explain their broad substrate specificity. Two additional features of the *TbTDPX2* structure, α 2 and the short loop α 2- β 5, share the same position as their equivalents in GPX4 (Figure 4), but, as can be seen in the oligomeric GPXs, these structural elements are involved in inter-subunit interfaces and are therefore determinants of the oligomerization state of this family. Interestingly, in the monomeric *TbTDPX2*, helix α 2 contains the resolving Cys87 as does the dimeric *PtGPX5*. However, in *PtGPX5* the dimer interface is different to those formed by the oligomeric selenocysteine-containing mammalian GPXs, and so the resolving cysteine of *PtGPX5* is not constrained by the interface [15].

Bipartite active site

The active site of mammalian GPXs is comprised of a well-conserved Cys, Gln and Trp catalytic triad [23]. Mutational studies in *TbTDPX3* suggests that Cys47 and Gln82 (equivalent to Cys39 and Gln74 in *TbTDPX2*) are essential for activity [11]. Mutation of Trp137 to a glycine, however, resulted in enzyme with low but significant activity suggesting that it plays a structural rather than a catalytic role [11]. Overlaying *TbTDPX2* with the other structurally described GPXs puts the triad components (Cys39, Gln74, Trp129; Figure 5A) in similar positions, but in *TbTDPX2* the distance between Cys39S γ and Gln74O ϵ 1 is on average 0.4 Å greater than the other homologues, whilst the distance between Cys39 and Trp129N ϵ 1 is on average 0.5 Å shorter.

One of the most unusual features of the reduced form of *TbTDPX2* is that the peroxidatic Cys39 and resolving Cys87 are situated 19 Å away from each other (Figure 3) and reside in distinct environments. The peroxidatic Cys39 is found in the loop connecting β 3- α 1 and, although this loop is solvent accessible, the side chain of Cys39 points towards the molecule's interior, as seen in the reduced structure of *PtGPX5* [15]. Cys39 is surrounded by Ala36, Tyr41, Gln74, Trp129, Asn130, and Phe131 that belong to loops β 3- α 1, β 4- α 2, and α 3- β 6 (Figure 5A). These residues are all conserved in the GPX family except Tyr41 which is specific to *TbTDPX2*. Cys39S γ accepts a hydrogen bond from Tyr41N (3.2 Å) and is 3.5 Å from Trp129N ϵ 1, 3.4 Å from Asn130N δ 2, and 3.9 Å from Gln74O ϵ 1. A water molecule sits 3.4 Å from Cys39S γ on the surface of *TbTDPX2*. Cys39N hydrogen bonds to Thr42OH, which is conserved in TDPXs and GPXs. It is not essential for catalysis [11], but

appears to stabilize the active site structure. Both Ala36 and Tyr41 are situated on the same loop (β 3- α 1) as Cys39. Analysis of a surface-charge representation (Figure 6A) shows that the active site region around Cys39 is not a well defined pocket or cleft. However, it lies in a predominantly positively charged region of the protein which may influence its substrate specificity.

The resolving Cys87 is situated at the C-terminus of helix α 2. It lies on the surface of the protein, is solvent accessible, and is situated at one end of a distinct pocket which is 14 Å long and 10 Å wide (Figure 6B). The base of the pocket is lined by residues Tyr20, Pro95, and Ile96 with Val86 immediately below Cys87 (Figure 5B). Down one side are the charged side chains of Lys18, Asp16, and Lys83. The opposite side is lined by main chain atoms of Ala92, Glu93, and Phe94, and a negatively charged patch of Asp78, Glu79, Glu80, Glu81, and Glu84 is seen on the electrostatic surface representation immediately above the charged side of the pocket. Cys87 does not directly interact with other residues in *Tb*TDPX2 in the reduced state. This is particularly unusual as it is situated in an α -helix, and whilst neighbouring residues follow the normal hydrogen-bonding pattern seen in such helices, Cys87 appears to remain non-bonded and flexible, suggesting its prerequisite for movement.

Possible mechanism and druggability

TDPXs are predicted to undergo significant conformational changes between their respective reduced and oxidized structures [11,13], as observed for *Pt*GPX5 [15]. A model based on oxidized *Pt*GPX5 (Figure 7) suggests that α 2 must completely unravel, causing loop β 4- α 2 to bulge outwards and allowing Cys87 to travel some 12 Å to form a disulphide bond with Cys39, which has itself moved 10 Å on the flexible β 3- α 11 loop. The trigger for this conformational change, which must reside in conversion of Cys39 thiolate to sulphenate, merits further investigation. These complex structural changes could explain the finite ping-pong mechanism found here by kinetic analysis (Figure 2 and Supplementary Figure S2) in contrast to the selenium type of glutathione peroxidases which lack the resolving cysteine and display an infinite k_{cat} .

Although the peroxidative Cys39 occupies a rather flat featureless surface in the reduced form, the environment of Cys87 forms a defined pocket that could be exploited for drug design (Figure 6). Likewise the model of the oxidised form predicts a deep pocket immediately above the disulphide bond (Figure 7). Both forms therefore present potentially druggable sites for small molecule inhibition. Structural studies on the oxidized form of *Tb*TDPX2 are necessary to confirm this prediction.

Acknowledgements

The authors thank Paul Fyfe and Scott Cameron for crystallographic data collection at the European Synchrotron Radiation Facility. This work is supported by the Wellcome Trust [grant numbers WT 079838; WT 083481].

References

- 1 Stuart, K. D., Brun, R., Croft, S. L., Fairlamb, A. H., Gurtler, R. E., McKerrow, J. H., Reed, S., and Tarleton, R. L. (2008) Kinetoplastids: related protozoan pathogens, different diseases. *J.Clin.Invest.* **118**, 1301-1310
- 2 Fairlamb, A. H. (2003) Chemotherapy of Human African Trypanosomiasis: Current and future prospects. *Trends Parasitol.* **19**, 488-494
- 3 Fairlamb, A. H. and Cerami, A. (1985) Identification of a novel, thiol-containing co-factor essential for glutathione reductase enzyme activity in trypanosomatids. *Mol.Biochem.Parasitol.* **14**, 187-198
- 4 Krieger, S., Schwarz, W., Ariyanayagam, M. R., Fairlamb, A. H., Krauth-Siegel, R. L., and Clayton, C. (2000) Trypanosomes lacking trypanothione reductase are avirulent and show increased sensitivity to oxidative stress. *Mol.Microbiol.* **35**, 542-552
- 5 Ariyanayagam, M. R., Oza, S. L., Guther, M. L., and Fairlamb, A. H. (2005) Phenotypic analysis of trypanothione synthetase knockdown in the African trypanosome. *Biochem.J.* **391**, 425-432
- 6 Comini, M. A., Guerrero, S. A., Haile, S., Menge, U., Lunsdorf, H., and Flohé, L. (2004) Validation of *Trypanosoma brucei* trypanothione synthetase as drug target. *Free Radic.Biol.Med.* **36**, 1289-1302
- 7 Comini, M. A., Krauth-Siegel, R. L., and Flohé, L. (2007) Depletion of the thioredoxin homologue tryparedoxin impairs antioxidative defence in African trypanosomes. *Biochem.J.* **402**, 43-49
- 8 Wilkinson, S. R., Horn, D., Prathalingam, S. R., and Kelly, J. M. (2003) RNA interference identifies two hydroperoxide metabolizing enzymes that are essential to the bloodstream form of the African trypanosome. *J.Biol.Chem.* **278**, 31640-31646
- 9 Hillebrand, H., Schmidt, A., and Krauth-Siegel, R. L. (2003) A second class of peroxidases linked to the trypanothione metabolism. *J.Biol.Chem.* **278**, 6809-6815
- 10 Schlecker, T., Schmidt, A., Dirdjaja, N., Voncken, F., Clayton, C., and Krauth-Siegel, R. L. (2005) Substrate specificity, localization, and essential role of the glutathione peroxidase-type tryparedoxin peroxidases in *Trypanosoma brucei*. *J.Biol.Chem.* **280**, 14385-14394
- 11 Schlecker, T., Comini, M. A., Melchers, J., Ruppert, T., and Krauth-Siegel, R. L. (2007) Catalytic mechanism of the glutathione peroxidase-type tryparedoxin peroxidase of *Trypanosoma brucei*. *Biochem.J.* **405**, 445-454
- 12 Wilkinson, S. R., Meyer, D. J., Taylor, M. C., Bromley, E. V., Miles, M. A., and Kelly, J. M. (2002) The *Trypanosoma cruzi* enzyme TcGPXI is a glycosomal peroxidase and can be linked to trypanothione reduction by glutathione or tryparedoxin. *J.Biol.Chem.* **277**, 17062-17071
- 13 König, J. and Fairlamb, A. H. (2007) A comparative study of type I and type II tryparedoxin peroxidases in *Leishmania major*. *FEBS J.* **274**, 5643-5658

- 14 Kabsch, W. (1993) Automatic processing of rotation diffraction data from crystals of initially unknown symmetry and cell constants. *J.Appl.Cryst.* **26**, 795-800
- 15 Koh, C. S., Didierjean, C., Navrot, N., Panjikar, S., Mulliert, G., Rouhier, N., Jacquot, J. P., Aubry, A., Shawkataly, O., and Corbier, C. (2007) Crystal structures of a poplar thioredoxin peroxidase that exhibits the structure of glutathione peroxidases: Insights into redox-driven conformational changes. *J.Mol.Biol.* **370**, 512-529
- 16 Vagin, A. and Teplyakov, A. (1997) MOLREP: an automated program for molecular replacement. *J.Appl.Cryst.* **30**, 1022-1025
- 17 CCP4 (1994) The CCP4 suite: programs for protein crystallography. *Acta Crystallogr.D* **50**, 760-763
- 18 Murshodov, G. (1997) Refinement of macromolecular structures by the maximum-likelihood method. *Acta Crystallogr.D* **53**, 240-255
- 19 Emsley, P. and Cowtan, K. (2004) Coot: model-building tools for molecular graphics. *Acta Crystallogr.D* **60**, 2126-2132
- 20 Dolinsky, T. J., Nielsen, J. E., McCammon, J. A., and Baker, N. A. (2004) PDB2PQR: an automated pipeline for the setup of Poisson-Boltzmann electrostatics calculations. *Nucleic Acids Res* **32**, W665-W667
- 21 Baker, N. A., Sept, D., Joseph, S., Holst, M. J., and McCammon, J. A. (2001) Electrostatics of nanosystems: application to microtubules and the ribosome. *Proc Natl Acad Sci U S A* **98**, 10037-10041
- 22 Holm, L. and Sander, C. (1996) Mapping the protein universe. *Science* **273**, 595-603
- 23 Epp, O., Ladenstein, R., and Wendel, A. (1983) The refined structure of the selenoenzyme glutathione peroxidase at 0.2-nm resolution. *Eur.J.Biochem.* **133**, 51-69
- 24 Kleywegt, G. J. and Jones, T. A. (1995) Where freedom is given, liberties are taken. *Structure.* **3**, 535-540
- 25 Schwede, T., Kopp, J., Guex, N., and Peitsch, M. C. (2003) SWISS-MODEL: An automated protein homology-modeling server. *Nucleic Acids Res* **31**, 3381-3385
- 26 Martin, J. L. (1995) Thioredoxin--a fold for all reasons. *Structure.* **3**, 245-250
- 27 Qi, Y. and Grishin, N. V. (2005) Structural classification of thioredoxin-like fold proteins. *Proteins* **58**, 376-388
- 28 Scheerer, P., Borchert, A., Krauss, N., Wessner, H., Gerth, C., Hohne, W., and Kuhn, H. (2007) Structural basis for catalytic activity and enzyme polymerization of phospholipid hydroperoxide glutathione peroxidase-4 (GPx4). *Biochemistry* **46**, 9041-9049

Table 1 Kinetic properties of TDPX with TryX as reducing agent and cumene hydroperoxide as substrate.

Data for *Tb*TDPX3 are from [9] fitted to the integrated Dalziel rate equation for a ping-pong mechanism. Data for *Lm*TDPX1 are from [13] fitted to the Michaelis-Menten equation for a ping-pong mechanism.

	k_{cat} [s ⁻¹]	K_{m} (CuOOH) [μM]	K_{m} (TryX) [μM]	k_1 (CuOOH) [M ⁻¹ s ⁻¹] x 10 ⁵	k_2 (TryX) [M ⁻¹ s ⁻¹] x 10 ⁵
<i>Tb</i> TDPX2*	38.3 ± 9.2	346 ± 88	69 ± 18	1.1 [†]	5.6 [†]
<i>Tb</i> TDPX2 [‡]	17 ± 4	80 [§]	25 [§]	2.2 ± 0.2	6.9 ± 0.5
<i>Tb</i> TDPX3	∞	∞	∞	1.0	2.1
<i>Lm</i> TDPX1	16.2	207	2.6	0.79	62

* Data from Figure 2 were globally fitted by non-linear regression using proportional weighting to the equation describing a ping-pong mechanism.

[†] Calculated from $k_{\text{cat}}/K_{\text{m}}$ values.

[‡] Data from Supplementary Figure S2 were analysed using the integrated Dalziel rate equation describing a ping-pong mechanism. Mean of two independent experiments.

[§] Calculated from $K_{\text{m}} = k_{\text{cat}}/k$.

Figure legends

Figure 1 Sequence-structure alignment of TDPXs and homologues

The protein sequences are accessible in the Swiss-Prot/TrEMBL databank under the following accession numbers: *T. brucei* TDPX2 (Q869A6), *T. brucei* TDPX1 (Q869A7), *T. brucei* TDPX3 (Q869A5), *L. major* TDPX1 (Q4Q9B2), poplar GPX5 (A3FNZ8) and human GPX4 (P36969). Secondary structure elements are colour-coded according to Figure 5 with α -helices in magenta, β -strands in cyan, and 3_{10} -helices in green. Residues identical in all sequences have been shaded in black, and those identical in most sequences are shaded in grey. Highlighted in yellow are the peroxidatic and resolving cysteines. The red circles denote the conserved active site triad residues. The different N- and C-termini of the three *Tb*TDPXs are shaded in red. The *Tb*TDPX2* sequence is that described in this study, and the mutational difference to the database sequence is highlighted by the blue star. The numbers at the end of each sequence correspond to the percent sequence identity to *Tb*TDPX2* in the alignment.

Figure 2 Kinetic analysis of TDPX2 with tryparedoxin and cumene hydroperoxide as substrate

(A) The initial velocities were determined with varied cumene hydroperoxide concentrations and different tryparedoxin concentrations (filled square: 12.5 μ M, open square: 10 μ M, filled circle: 7.5 μ M, open circle: 5 μ M). The initial velocities for each individual data set were initially fitted individually to the Michaelis-Menten equation (dotted line) by non-linear regression using GraFit and subsequently the entire data set globally fitted to the equation describing a ping-pong mechanism (solid line).

(B) The reciprocal V_{\max}^{app} data, calculated for each TryX concentration data set, were plotted against the reciprocal tryparedoxin concentrations. The reciprocal intercept represents the reciprocal V_{\max} value and the reciprocal slope the rate constant k_2 for TryX.

(C) The reciprocal initial velocities are plotted against the reciprocal cumene hydroperoxide concentrations. This Figure shows the accuracy of the two fits transformed as a Lineweaver-Burk plot (solid line: global fit, dotted line: individual fits for each tryparedoxin concentration). The slope represents the reciprocal rate constant k_1 for cumene hydroperoxide. Kinetic constants are reported in Table 1.

Figure 3 Ribbon diagram of *Tb*TDPX2 with secondary structure elements labelled

α -Helices are magenta, β -strands are cyan, and 3_{10} -helices (θ_1 and θ_2) are shown in green. The peroxidatic and resolving cysteine side chains are shown as sticks. See text for further details.

Figure 4 Panel showing $\text{C}\alpha$ backbone representations of *Tb*TDPX2, hGPX4 and bGPX1

Circled in yellow is helix α_2 from each structure, showing the similarity between the monomeric *Tb*TDPX2 and human GPX4 and their difference to bovine GPX1. Circled in blue is the loop α_3 - β_6 which is the same length in hGPX4, though taking on a slightly different conformation, and markedly different in bGPX1. This loop is involved in dimer interface interactions in the oligomeric GPXs, and may also regulate substrate specificity.

Figure 5 Detailed stick representation of (A) the peroxidatic and (B) resolving cysteine environments

Important residues have been labelled and are discussed in the text. Oxygen atoms are depicted in red, nitrogen atoms in blue, sulphur atoms in yellow, and carbon atoms in cream.

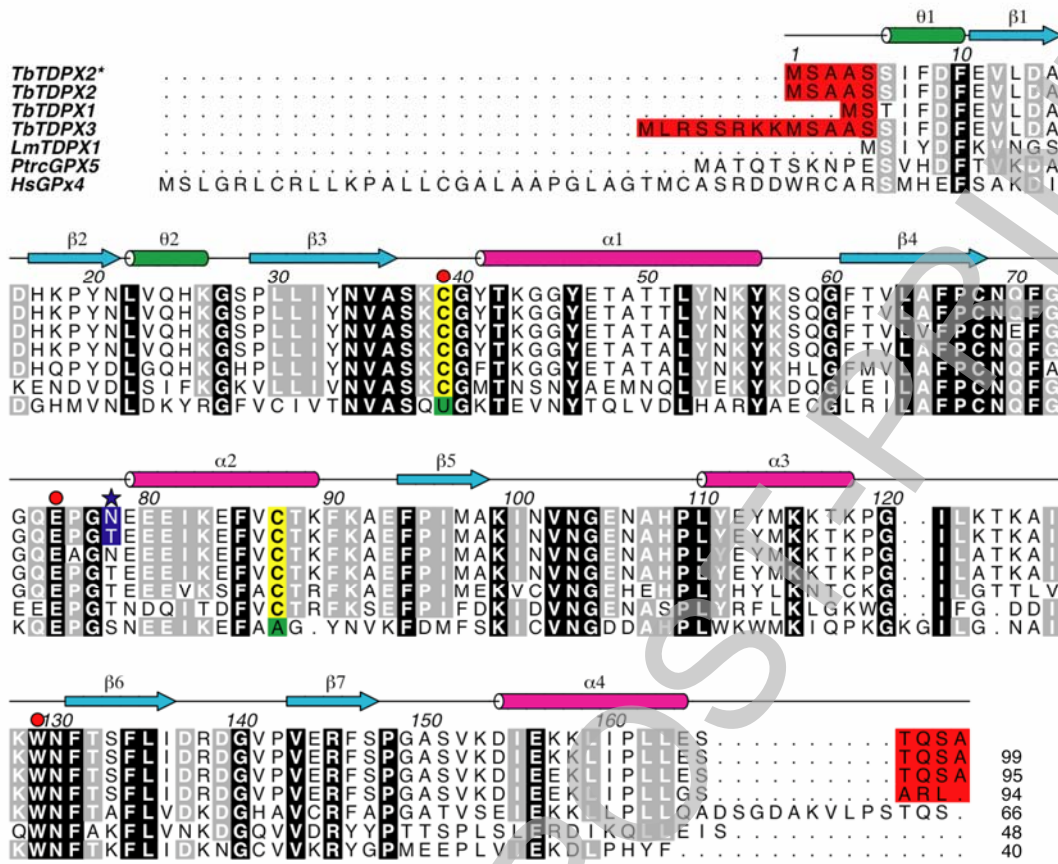
Figure 6 Surface electrostatic potential representation of *Tb*TDPX2

Positive charge is shown as blue and negative charge as red. Panel A shows the positively charged region surrounding the peroxidatic Cys39 with other residues marked as a guide to orient with other figures. Panel B shows the enzyme rotated 90° along the y-axis to reveal the environment surrounding the resolving Cys87. The pocket below Cys87 can clearly be seen, as can the negatively charged Glu-rich region above the pocket.

Figure 7 Ribbon and surface potential representations of the model of oxidized *Tb*TDPX2 based on *Pt*GPX5

In the ribbon diagram, the loop containing Cys39 is coloured red, that containing Cys87 is orange, and the disulphide between the two cysteines is shown as sticks. The electrostatic surface representation shows the position of the disulphide and how the structural changes associated with oxidation generate surface features that may be of value in the design of enzyme inhibitors, for example the deep pocket created immediately above the disulphide bond, the base of which is lined by Phe85, with a negatively charged lid of Glu80 and Glu81.

Figure 1



THIS IS NOT THE FINAL VERSION - see doi:10.1042/BJ20080889

Stage 2(a) FINAL

Figure 2

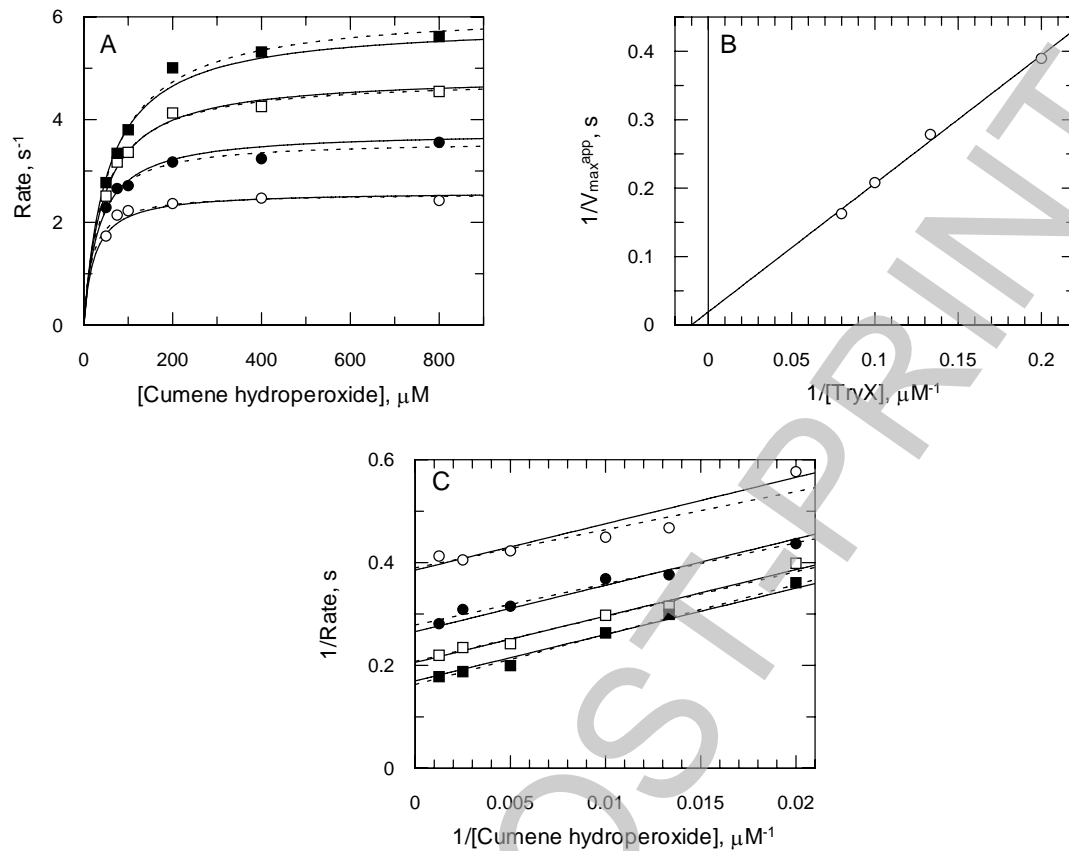


Figure 3

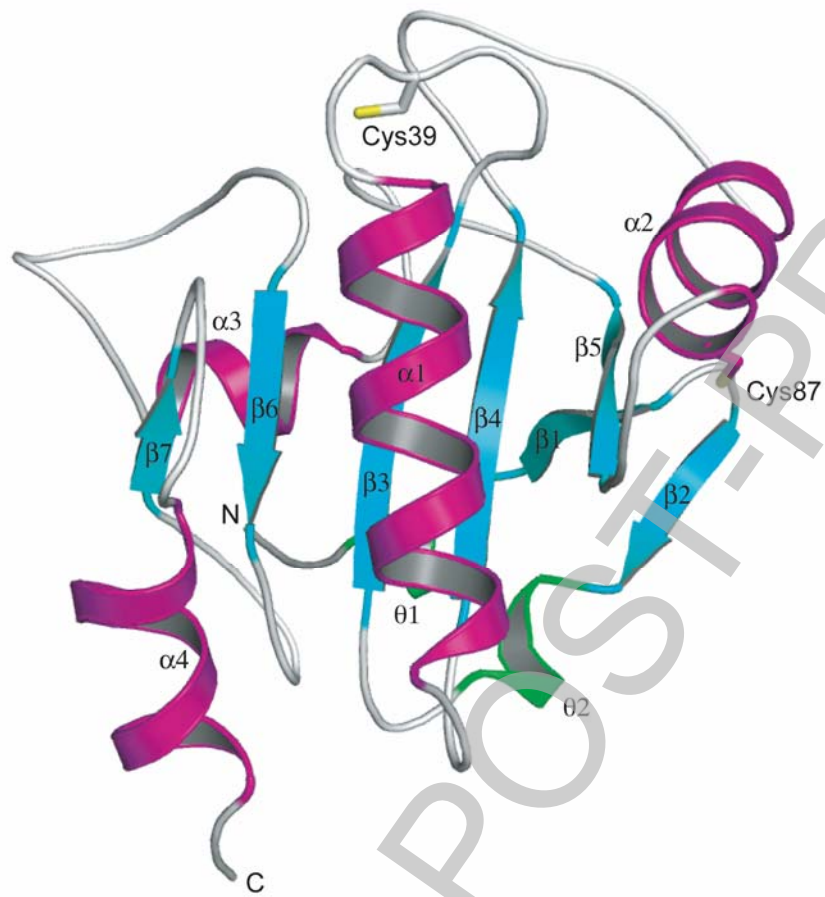


Figure 4

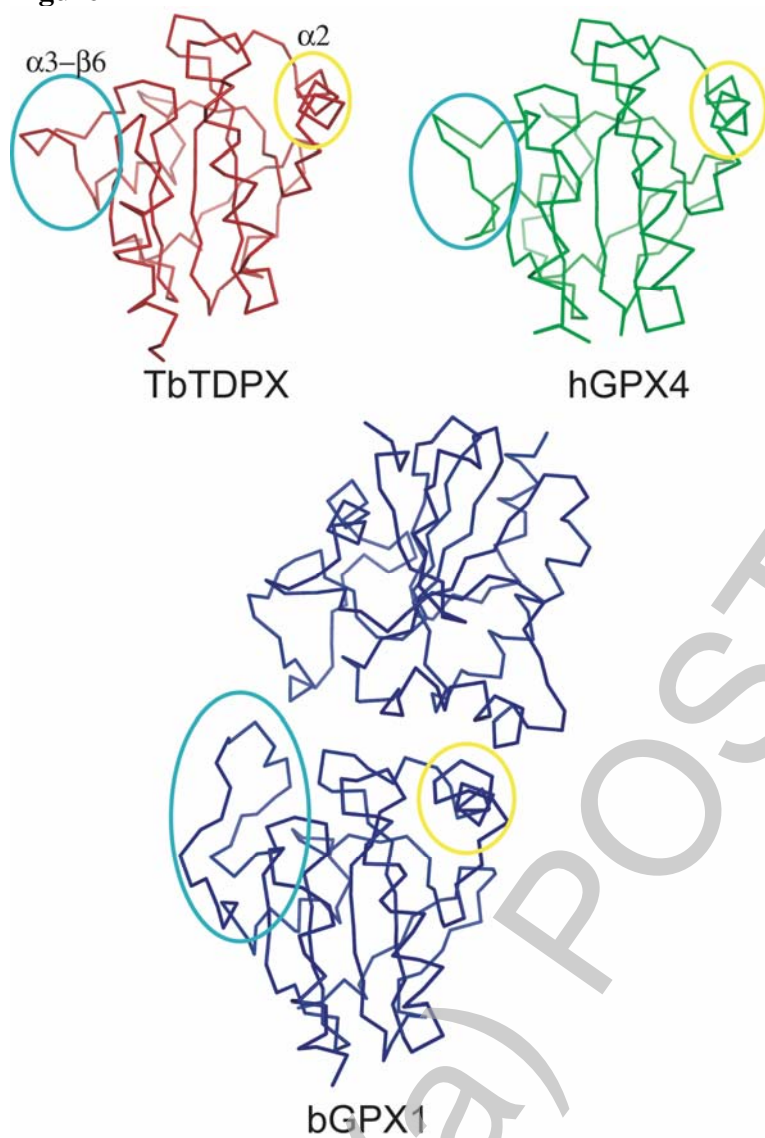


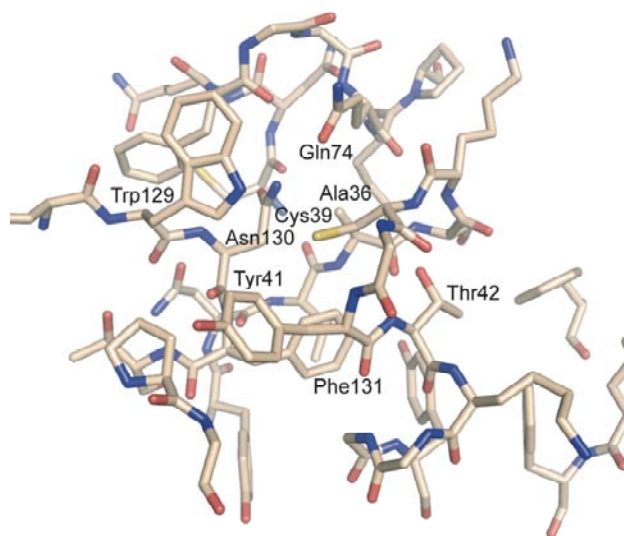
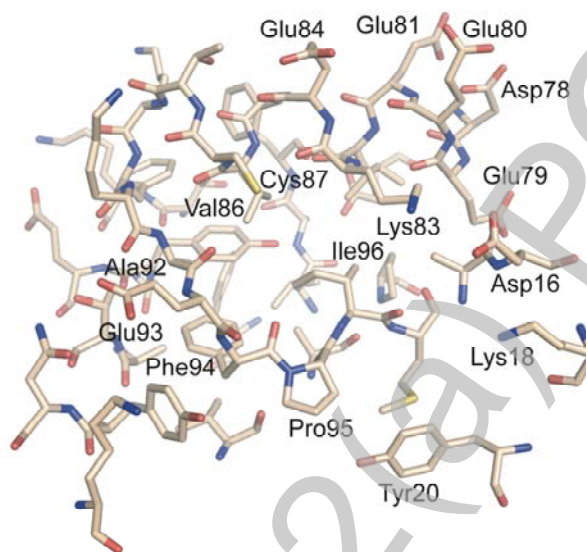
Figure 5A**Figure 5B**

Figure 6

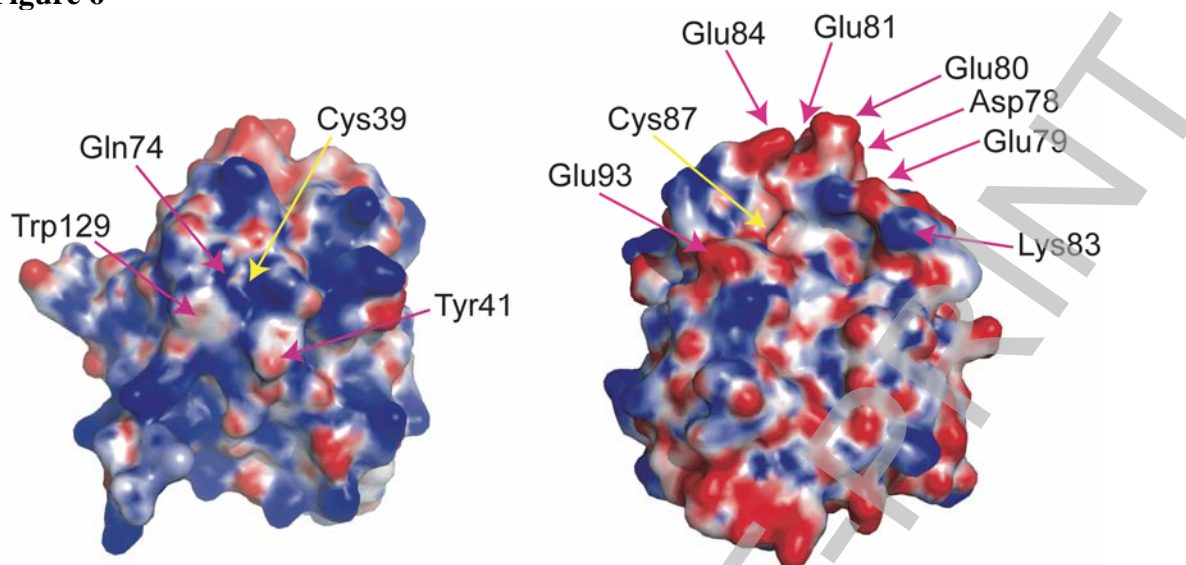
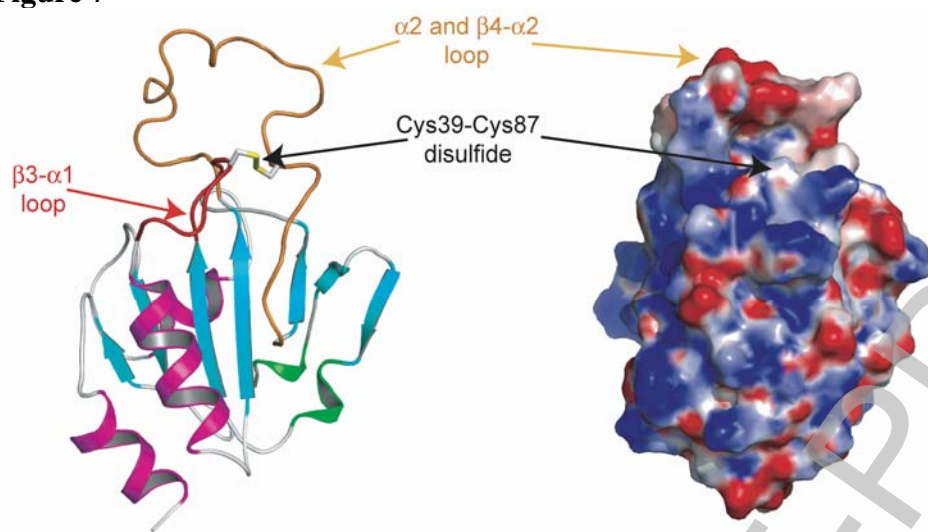


Figure 7



Stage 2(a) POST-PRINT